AGU PUBLICATIONS

Geophysical Research Letters

RESEARCH LETTER
10.1002/2017GL075735

Key Point:
- Aerial thermal imagery collected at Gulf Stream's boundary reveals fine structure of the front's breakdown due to symmetric instability

Supporting Information:
- Supporting Information S1

Correspondence to:
I. Savelyev,
ivan.savelyev@nrl.navy.mil

Citation:
Savelyev, I., Thomas, L. N., Smith, G. B., Wang, Q., Shearman, R. K., Haack, T., … Fernando, H. J. S. (2018). Aerial observations of symmetric instability at the North Wall of the Gulf Stream. *Geophysical Research Letters*, *45*, 236–244. https://doi.org/10.1002/2017GL075735

Received 18 SEP 2017
Accepted 24 NOV 2017
Accepted article online 1 DEC 2017
Published online 8 JAN 2018

Aerial Observations of Symmetric Instability at the North Wall of the Gulf Stream

I. Savelyev[1], L. N. Thomas[2], G. B. Smith[1], Q. Wang[3], R. K. Shearman[4], T. Haack[5], A. J. Christman[6], B. Blomquist[7], M. Sletten[1], W. D. Miller[1], and H. J. S. Fernando[6]

[1]Remote Sensing Division, U.S. Naval Research Laboratory, Washington, DC, USA, [2]Department of Earth System Science, Stanford University, Stanford, CA, USA, [3]Department of Meteorology, Naval Postgraduate School, Monterey, CA, USA, [4]College of Earth, Ocean, and Atmospheric Sciences, Oregon State University, Corvallis, OR, USA, [5]Marine Meteorology Division, US Naval Research Laboratory, Monterey, CA, USA, [6]Department of Civil and Environmental Engineering and Earth Sciences, University of Notre Dame, South Bend, IN, USA, [7]Earth System Research Laboratory, National Oceanic and Atmospheric Administration, Boulder, CO, USA

Abstract An unusual spatial pattern on the ocean surface was captured by thermal airborne swaths taken across a strong sea surface temperature front at the North Wall of the Gulf Stream. The thermal pattern on the cold side of the front resembles a staircase consisting of tens of steps, each up to ~200 m wide and up to ~0.3°C warm. The steps are well organized, clearly separated by sharp temperature gradients, mostly parallel and aligned with the primary front. The interpretation of the airborne imagery is aided by oceanographic measurements from two research vessels. Analysis of the in situ observations indicates that the front was unstable to symmetric instability, a type of overturning instability that can generate coherent structures with similar dimensions to the temperature steps seen in the airborne imagery. It is concluded that the images capture, for the first time, the surface temperature field of symmetric instability turbulence.

1. Introduction

While the dominant sources of kinetic energy (KE) of the ocean circulation are well known, that is, the tides and winds, and their rates of energy input have been quantified, the sinks of KE are diverse and not fully understood (Ferrari & Wunsch, 2009). Processes that are responsible for KE dissipation break the tendency of the geostrophically balanced circulation and provide a mechanism of energy transfer between small and large scales. Therefore, it is critical to resolve them in order to close the KE budget of the circulation. Submesoscale instabilities are thought to play an important role in this regard since their dynamics is less constrained by the Earth's rotation, allowing them to facilitate a forward energy cascade to small scales where viscous dissipation can act (McWilliams, 2016). One such submesoscale instability that has been observed to be effective at dissipating the KE in balanced flows is symmetric instability (SI) (D'Asaro et al., 2011; Thomas et al., 2016). SI forms in the surface boundary layer of ocean fronts under destabilizing atmospheric forcing associated with surface buoyancy loss and/or down-front winds (Thomas, 2005). SI does not, however, derive its energy from this atmospheric forcing but instead feeds off the KE in the thermal wind shear and thus represents a sink of KE for the circulation (Taylor & Ferrari, 2010; Thomas & Taylor, 2010; Thomas et al., 2013). SI turbulence is hence a unique form of boundary layer turbulence in that the standard sources of turbulent kinetic energy, winds, air-sea buoyancy fluxes, and surface gravity waves, do not contribute directly to its energetics.

SI turbulence is characterized by overturning cells that tilt parallel to the slanted isopycnals of a front and align longitudinally with thermal wind shear (Taylor & Ferrari, 2010). These coherent structures also impart a signature in the surface density field, as their near-surface circulation resorts the lateral density distribution of a front, organizing it into a series of steps (Thomas, 2005). The distance between steps is equal to the width of the SI overturning cells, L_{SI}, which scales as the boundary layer depth, H, over the isopycnal slope, s_ρ (Thomas & Lee, 2005). The isopycnal slope in the surface boundary layers of ocean fronts is typically small, ranging from 0.01 to 0.1, because lateral density gradients tend to keep the boundary layer stratified (Thomas et al., 2013). Hence, the aspect ratio of SI overturning cells, H/L_{SI}, is much less than one.

Roll vortices in the boundary layer can exhibit complex, chaotic behavior. Langmuir cells, for example, have been modeled and observed to develop longitudinal variations and defects (Farmer & Li, 1995; McWilliams et al., 1997; Smith, 1998). It has not been investigated observationally whether the coherent structures of SI follow similar behavior, as previous observational studies of SI (e.g., D'Asaro et al., 2011; Thomas et al., 2016) were not designed to characterize the three-dimensional nature of its turbulence. In this article we describe high-resolution, airborne sea surface temperature imagery of the North Wall of the Gulf Stream made when the current was symmetrically unstable. The imagery reveals in great detail the spatial variations of coherent structures thought to be associated with SI.

2. Methods

2.1. Experiment

The observations presented here were collected as a part of a larger experiment CASPER-East (Wang et al., 2017) conducted for the Office of Naval Research MURI "Coupled Air-Sea Processes and Electromagnetic wave ducting Research." The experiment was conducted in October and early November 2015, primarily over the shelf, off the coast of North Carolina with a 3 day long excursion to the nearby Gulf Stream boundary on 30 October to 1 November. The airborne imagery presented in this paper were collected by a research aircraft as a part of the Gulf Stream scouting flight on the evening of 29 October a few hours before both research vessels entered the area. Tracks of the aircraft and of both research vessels as they enter the Gulf Stream for the first time are shown in Figure 1. The aircraft's objective was to fly in a zigzag pattern to cross the Gulf Stream's North Wall multiple times and thus map the location and shape of the primary sea surface temperature (SST) front. The resulting thermal map was transmitted to research vessels within hours after the flight to help establish their sampling strategy. Airborne observations that this paper highlights were collected as an unintended by-product of the scouting zigzag flight. Relevant segments of data sets obtained by other means are also presented to clarify larger-scale meteorological and oceanographic conditions and thus aid in interpretation of airborne imagery.

2.2. Remote Sensing Aircraft SAAB 340

For the purposes of this experiment a SAAB 340 aircraft was equipped with a wide variety of high-resolution ocean imagers, including active or passive sensors in visible, infrared, and microwave bands. Thermal imagery of the ocean surface presented below were collected by a passive midwave (3–5 μm) infrared camera FLIR SC6000. Image geolocation was made possible via a high-grade aircraft positioning system C-MIGITS. The resulting spatial resolution of ocean surface imagery was ~1 × 1 m per pixel with ~1–2 m absolute pixel geolocation accuracy. The infrared camera was calibrated in laboratory conditions against a controlled temperature black body resulting in a thermal sensitivity of ~0.02 K. In field conditions various unknown factors, such as camera lens temperature variations, sky reflectance, and atmospheric absorption tend to introduce a bias to SST estimates. The bias was removed using collocated in situ SST measurements collected by R/V *Sharp*.

2.3. R/V *Sharp*

In addition to a standard underway flow through thermistor with an intake at 1 m depth, R/V *Sharp* measured SST using an on board Infrared SST Autonomous Radiometer (ISAR) probe. This measurement gave the most accurate value of skin SST among all CASPER assets and was used as a reference point for other SST estimates (Alappattu, Wang, Yamaguchi, Lind, Reynolds, et al., 2017; Alappattu, Wang, Yamaguchi, Lind, Christman, et al., 2017).

2.4. R/V *Atlantic Explorer*

Similar to R/V *Sharp*, R/V *Atlantic Explorer* (R/V *AE*) measured bulk SST and salinity using a flow through system with the intake at ~2 m below the water surface. A down looking acoustic Doppler current profiler provided underway vertical profiles of horizontal velocity down to ~300–500 m depth. A suit of sensors installed on a bow mast collected standard meteorological measurements, which were used as inputs for COARE 3.5 bulk flux algorithm (Edson et al., 2013) to estimate sensible and latent heat fluxes as well as the wind stress.

Over a ~24 h period after the first crossing of the Gulf Stream boundary, R/V *AE* made a total of 11 conductivity-temperature-depth (CTD) casts on both sides of the SST front with ~5 km spacing between stations (see tracks in Figure 1). Each CTD station sampled the temperature and salinity down to 300 m.

2.5. COAMPS Numerical Model

A high-resolution version of the U.S. Navy's Coupled Ocean/Atmosphere Mesoscale Prediction System (COAMPS) was setup to provide operational support to the CASPER-East experiment. The atmospheric

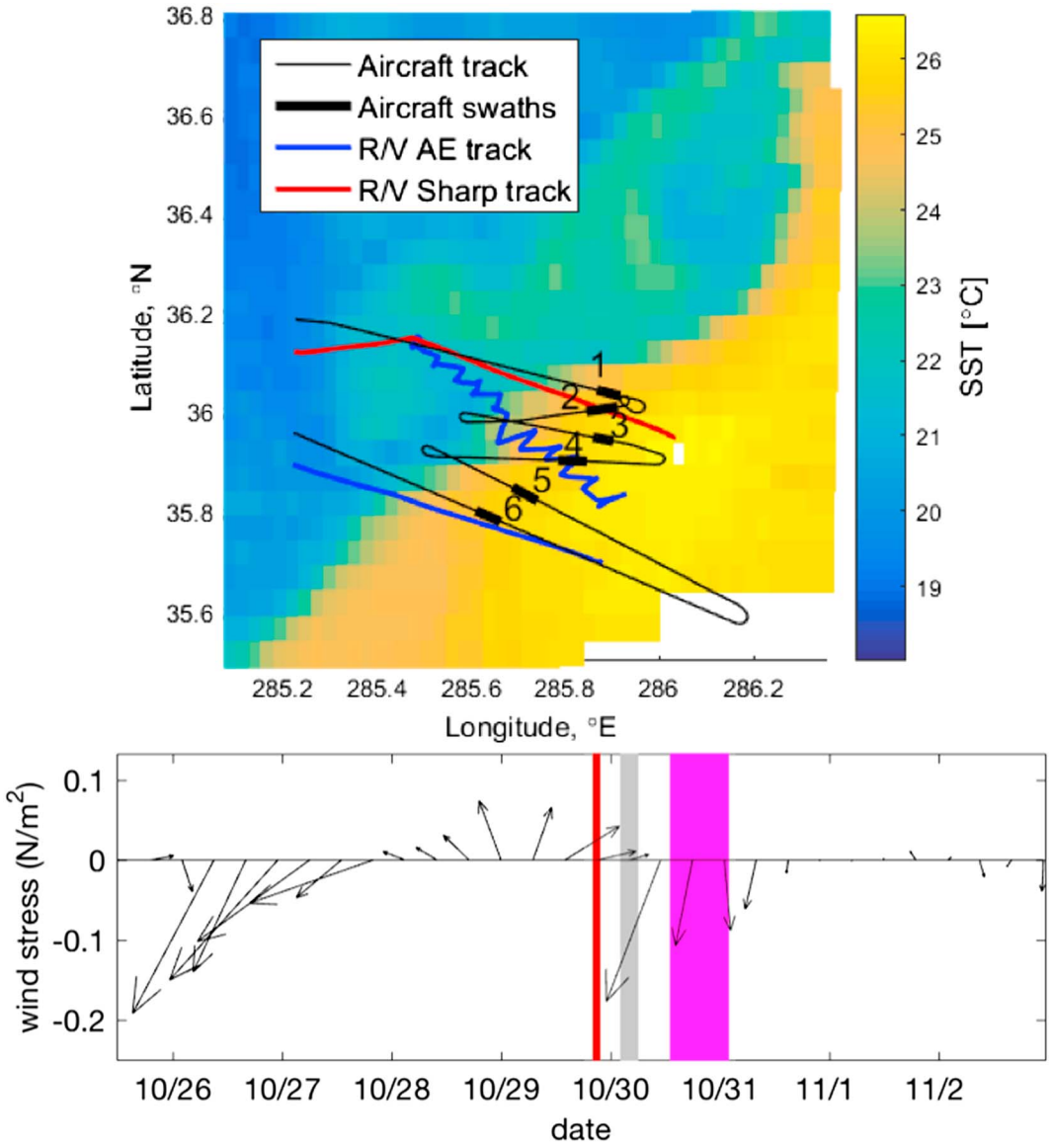

Figure 1. (top) GOES 13 geostationary satellite SST image of the study area on 30 October 2015 and the track of the aircraft (thin black), R/V *Sharp* (red), and R/V *Atlantic Explorer* (blue). The locations of the airborne SST swaths shown in Figure 2 are indicated with the thick black lines. The R/V *Atlantic Explorer* first crossed the front south of 36°N and on its second crossing further to the north completed the hydrographic section. (bottom) Time series of the wind stress vector from the Coupled Ocean/Atmosphere Mesoscale Prediction System (COAMPS) model, spatially averaged over the study area. The times when the airborne imagery (Figure 2), underway data (Figure 3), and hydrographic section (Figure 4) were made are indicated in Figure 1 (bottom) with the shaded areas in red, gray, and magenta, respectively.

component of COAMPS had 70 terrain following vertical levels and an inner nest with 2 km horizontal grid spacing, while the oceanic component (NCOM) spanned 50 levels with an inner nest of 3 km horizontal grid spacing. Initial and lateral boundary conditions were supplied by the Navy's global operational models (NAVGEM for the atmosphere and HYCOM for the ocean), and every 6 h the model fields were updated with local observations. Complete details of COAMPS modeling components, the coupled modeling framework, and data assimilation, analysis, and forecast workflow are given by Chen et al. (2003).

3. Results

The field campaign was conducted around the North Wall of the Gulf Stream at a time when its main SST front was nominally aligned from the southwest to the northeast, see SST map in Figure 1 obtained

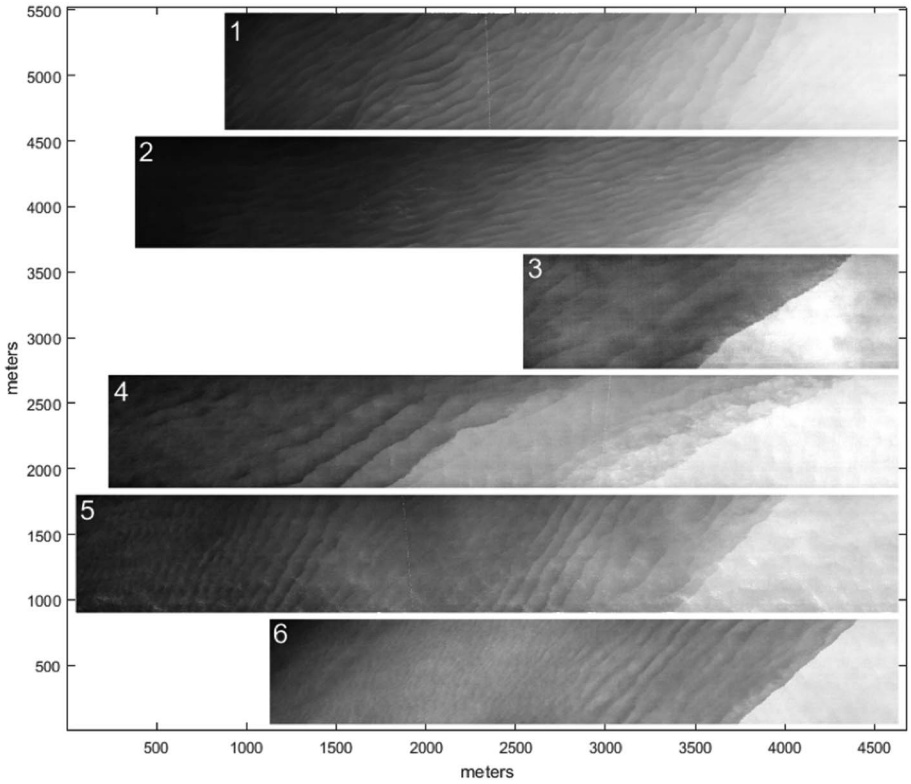

Figure 2. Six infrared swaths across the primary Gulf Stream front. Each swath demonstrates the staircase phenomenon on the cold (i.e., dark) side of the front. Image color represents sea surface temperature, normalized for each swath to maximize contrast. The range of temperatures (°C) shown varies between swaths as follows, 1: 22.2 to 25.4, 2: 22.3 to 24.9, 3: 24.9 to 25.9, 4: 24.5 to 26.1, 5: 24.4 to 26.3, and 6: 23.9 to 25.8.

by the geostationary satellite GOES13. The front was complicated by several submesoscale features in the flow, specifically a streamer of warm Gulf Stream water north of the front that was separated from the main current by a filament of cold water, features that are commonly found near the North Wall (e.g., Klymak et al., 2016). Prior to the experiment there was a strong wind event with winds directed to the southwest, which then weakened and rotated clockwise approximately 24 h prior to the flight (Figure 1, bottom). At the time of the aircraft survey, the wind stress had reduced substantially, but then subsequently strengthened as the research vessels arrived at the field site.

The aircraft flight track crossed the main SST front at every leg of the zigzag pattern seen in Figure 1 with each crossing numbered from 1 to 6. The high-resolution thermal imagery swaths collected by the aircraft at each of the six crossings are shown in Figure 2. While distances are preserved within each swath, rotation angles and relative locations are changed in order to stack the imagery. Thermal contrast is also normalized separately for each image in order to maximize the visibility of observed structures. Bright color on the right side of each image corresponds to the warm core temperature of the Gulf Stream, whereas darker color on the left is colder waters on the other side of the front. The focal point of this paper is the multistep "staircase" transition structure from warm to cold water apparent on each of the six swaths. This highly organized staircase pattern with $\mathcal{O}$(100 m) spatial and up to ~0.3°C thermal steps is unexpected, as opposed to a more chaotic turbulent transition pattern, or a more uniform gradient, or a single sharp step. Note that this staircase structure appeared only at the warm end of the otherwise smooth wider temperature gradient seen in the satellite imagery.

Shortly after the aircraft survey, R/V *AE* collected oceanographic observations across the same front, which consisted of underway temperature and salinity measurements and shipboard acoustic Doppler current profiler (ADCP) velocity profiles (Figures 3a, 3c, and 3e). These observations provide information on how the temperature fields seen in the satellite and airborne imagery (Figures 1 and 2) are related to density and velocity, the variables that are most relevant for the hydrodynamic instabilities that could be responsible

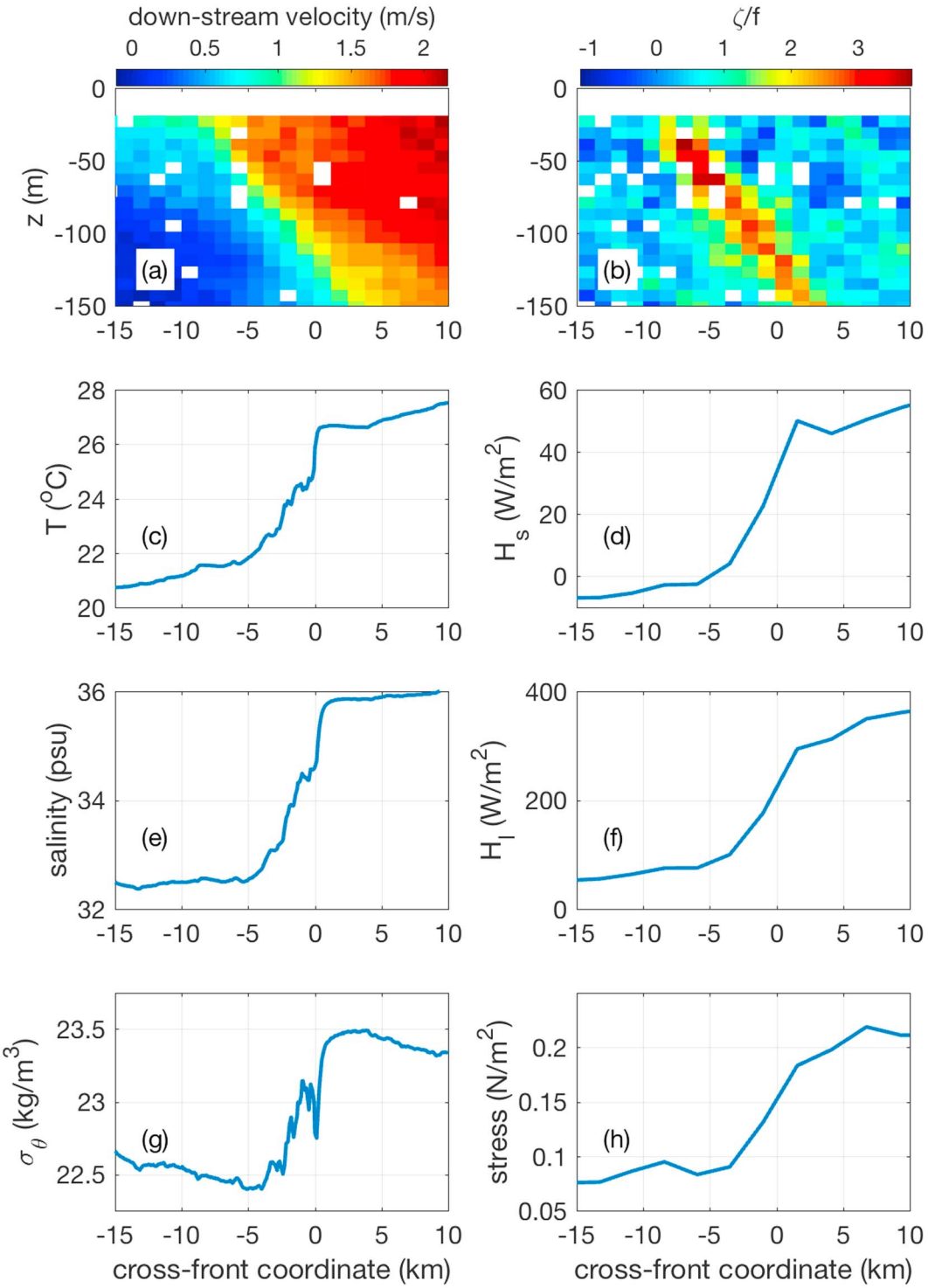

Figure 3. Velocity profiles and underway meteorological and oceanographic measurements collected by R/V *Atlantic Explorer* while crossing the SST front on its southernmost leg (Figure 1). (a) The downstream component of the velocity v_{df}. (b) An estimate of the vertical vorticity $\zeta = \partial v_{ds}/\partial \hat{x}$ normalized by f. Underway measurements of (c) temperature, (e) salinity, (g) potential density, (d) fluxes of sensible, (f) latent heat, and (h) wind stress.

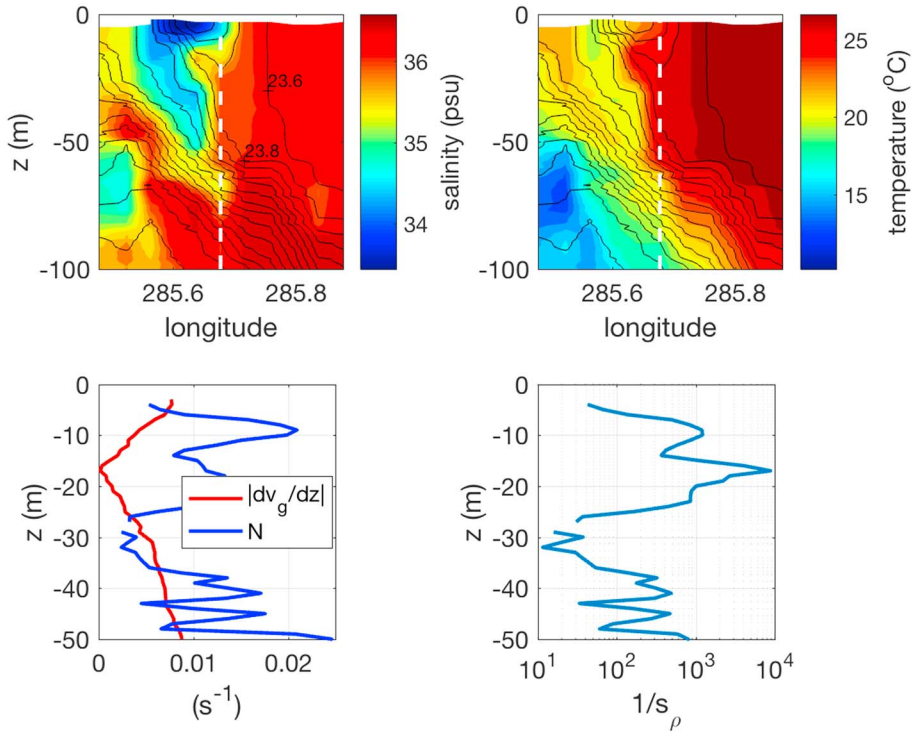

Figure 4. (top row) Sections of (left) salinity and (right) temperature crossing the Gulf Stream front and the cold, fresh filament. Isopycnals are contoured at an interval of 0.2 kg m^{-3}. (bottom lower) Profiles of the stratification (blue) and the magnitude of the thermal wind shear (red) on the eastern edge of the cold, fresh filament where the staircase was observed (at the location indicated by the dashed white line in Figure 4 (top row)). (bottom right) Profile of the inverse of the isopycnal slope at that same location.

for the SST staircase. To facilitate interpretation, velocities were projected into a down-front/cross-front coordinate system with axes parallel and perpendicular to the velocity vector of the Gulf Stream at its peak speed. A section of the down-front component with velocity v_{df} (Figure 3a) shows the vertical tilt of the North Wall with faster Gulf Stream water leaning over the slower shelf water resulting in strong lateral and vertical shears. The lateral shear can be used to estimate the vertical vorticity as $\zeta = \partial v_{df}/\partial \hat{x}$ ($\hat{x}$ is the cross-front coordinate that starts at the temperature front and increases moving toward warmer waters). A sheet of positive vorticity with values exceeding the Coriolis parameter, f, delineates the North Wall and extends up to the surface, outcropping at a distance of about 10 km from the front (Figure 3b).

The flow through temperature observations (Figure3c) highlight the strong ~4°C temperature front where the staircase was observed. Despite this large temperature drop, the density of the water (Figure 3g) actually *decreases* by ~1 kg m^{-3} as the result of a ~3 practical salinity unit drop in salinity (Figure 3e). This cool, fresher water is a manifestation of the cold filament evident in the satellite SST image (Figure 1). Hydrographic casts taken a day later reveal that the cold filament is a relatively shallow feature of order 10 m thick (Figure 4, top left). From the western end of the filament, a plume of low-salinity water extends along isopycnals down to ~50 m, evidencing active subduction. West of this plume the surface waters become warmer (Figure 4, top right), consistent with the structure of the SST seen in the satellite image (Figure 1). The warming occurs where the pycnocline reconnects to the surface having been split from the main branch of the Gulf Stream by the cold filament.

4. Discussion

Observations of the staircase structure shown in Figure 2 are very unusual even for an experienced aerial infrared ocean observer. To the best of our knowledge such structures have not been reported in the literature, especially combined with supporting in situ measurements. In this section we present a discussion on what might be causing the staircase.

First, variations in surface reflectivity due to surface waves have to be ruled out as the cause of the staircase signal, since waves also possess a spatial pattern with regular banding. This was verified by analyzing raw infrared video files collected at 60 Hz, which provide ~10–20 s dwell time over any given location as it passes through the field of view. Within this dwell time surface waves were observed due to some sun glint along the crests. Waves were seen to have similar wavelength as the staircase but oriented in a different direction and propagating relatively quickly, while the staircase remained stationary. More importantly, the staircase was only observed near the SST front, whereas if this signal was due to surface waves, it would have been seen everywhere.

A second hypothesis might be that the staircase exists throughout the ocean surface but is only detected near the SST front, because the front supplied an ample temperature signal to be detected by the infrared camera. As a potential candidate, Langmuir cells aligned with the front could organize a smooth SST gradient into a series of steps. In this scenario, sharp temperature steps would arise due to mixing barriers that form between pairs of cells. This argument is supported by the fact that the wind was approximately aligned with the front during the aircraft survey. However, with mixed layer depth of ~10 m, the ~100 m width of the steps is not consistent with the order one aspect ratio characteristic of Langmuir cells (Smith et al., 1987). This same argument rules out roll vortices due to inflection-point instabilities (Etling & Brown, 1993).

Third, the staircase might be a footprint of an atmospheric process associated with the sharp SST front. Indeed, air-sea fluxes shown in Figures 3d, 3f, and 3h undergo a rapid transition near the front, indicating a regime change in the atmospheric boundary layer turbulence. This topic is of interest on its own merits and is a subject of a separate paper currently in preparation. One indication that the staircase is probably not merely a footprint of an atmospheric process is that the staircase appears to be associated with strong salinity fluctuations (Figure 3e), which the atmosphere cannot cause directly.

A fourth possibility is that the temperature steps are a manifestation of a frontal instability. The fact that the steps form within ~5 km of the SST front where the lateral density gradient is strong (Figure 3g) supports this hypothesis. The particular frontal instability that seems the most likely candidate is SI, given the symmetric nature (i.e., invariance in the along-front direction) of the staircase. This hypothesis can be tested more quantitatively by calculating the instability criteria for SI. A front is symmetrically unstable when the Richardson number of the geostrophic flow, $Ri_g = N^2/(\partial v_g/\partial z)^2$, satisfies the following:

$$Ri_g < \frac{1}{1+\zeta/f} \tag{1}$$

(Haine & Marshall, 1998), where $N^2 = -(g/\rho)\partial\rho/\partial z$ is the square of the buoyancy frequency, and

$$\frac{\partial v_g}{\partial z} = -\frac{g}{f\rho}\frac{\partial \rho}{\partial \hat{x}} \tag{2}$$

is the thermal wind shear at the front (g is the acceleration due to gravity and ρ is the density).

Criterion (1) was evaluated using the observations at the front where the staircase was observed. At this location, the boundary layer depth (as defined as the depth below which $Ri_g > 1$) is quite shallow, $H \sim 5$ m, because of the stratification in the cold filament. Within this boundary layer, the thermal wind shear exceeds N, yielding $Ri_g < 1$ (Figure 4, bottom left). While we do not have direct observations of ζ near the surface (since the ADCP measurements start at 25 m), integrating the thermal wind shear to yield a geostrophic estimate for the vorticity suggests that $|\zeta|/f = \mathcal{O}(0.1)$ in the boundary layer and thus the front satisfies criterion (1) for SI.

An additional factor to consider for wind-forced symmetrically unstable fronts is that the wind stress, τ, must be weak enough for SI to dominate over standard wind-driven turbulence in the boundary layer, specifically

$$\frac{\tau}{\rho(\partial v_g/\partial z)^2 H^2} \ll 1 \tag{3}$$

(Thomas et al., 2013). At the time when the airborne SST image was made, the wind stress was ~0.04 N m^{-2}, which given the boundary layer depth $H \sim 5$ m, and thermal wind shear $|\partial v_g/\partial z| \sim 0.007$ s^{-1} (Figure 4, bottom left) is sufficiently weak to satisfy (3). The criterion is also satisfied using the value of the wind stress averaged over the previous 5 days, that is, 0.1 N m^{-2}, when the winds were stronger.

Further evidence that the temperature staircase is associated with SI comes from comparing the width of the temperature steps to the theoretical prediction. According to the theory for SI, the width of SI cells is $L_{SI} = H/s_\rho$, where s_ρ is the slope of isopycnals in the boundary layer (Thomas, 2005). For the isopycnal slope in the front

(Figure 4, bottom right), $L_{SI} \sim 200$ m in the top 5 m, a spacing consistent with the observed temperature steps.

Another consideration to take into account is whether the atmospheric forcing was conducive to the formation of SI. Down-front winds and/or air-sea heat loss can drive frontal currents symmetrically unstable and both types of forcing were active over the cold, fresh filament. Latent and sensible heat fluxes during the underway survey were destabilizing, resulting in a heat loss of order 100 W m^{-2} (Figures 3d and 3f). Contrarily, daytime downwelling shortwave radiation can exceed this value by a few hundred W m^{-2}. In addition, the strong winds blowing to the southwest from 26 to 28 October (Figure 1) were down-front at the main SST front since the lateral density gradient was reversed by the filament (Figure 3g). However, just prior to the airborne SST measurements, the winds rotated ~180°, which could have stabilized the front. To quantify the net effect of the wind forcing on the front, the time-averaged cross-front Ekman transport, $\bar{U}_{cf}$, was calculated to determine if it was in the sense to advect denser water over light and drive SI (see supporting information). During the time when the airborne imagery was taken $\bar{U}_{cf} \approx -0.5$ m^2 s^{-1}, that is, the net effect of the winds was to destabilize the front. When acting on the lateral density gradient of the filament (e.g., Figure 3g), this transport results in a time-averaged Ekman buoyancy flux, $\overline{\mathrm{EBF}} = -(g/\rho)\bar{U}_{cf}\partial\rho/\partial\hat{x} \sim 1 \times 10^{-6}$ W kg^{-1}, that can drive turbulence equivalent to $\sim 2,000$ W m^{-2} of heat loss that could have easily created a symmetrically unstable flow at the front (Thomas et al., 2016).

5. Conclusion

A striking staircase-like feature in SST was observed in high-resolution infrared imagery of the Gulf Stream front and was likely caused by coherent structures associated with SI turbulence in the surface boundary layer. This conclusion was reached for several reasons. In situ observations of density indicate that the front satisfied the instability criteria for SI. Furthermore, the atmospheric forcing leading up to the staircase was conducive for driving SI by the action of down-front winds. Finally, the width of the temperature steps in the staircase is consistent with the expected size of SI overturning cells, yet an order of magnitude larger than roll structures associated with other forms of boundary layer turbulence such as Langmuir cells and inflection-point instabilities, which have order 1 aspect ratios. The airborne imagery suggests that while differing from these other forms of boundary layer turbulence in aspect ratio, SI turbulence appears to be characterized by similar types of longitudinal variability. While the temperature steps are coherent over several step widths in the longitudinal direction, they do show fluctuations in width and can form defects such as *Y* junctions (e.g., Figure 2 near 2,000 m in swath 4) a feature that is regularly seen in Langmuir turbulence (Farmer & Li, 1995; McWilliams et al., 1997). Such longitudinal variations in SI turbulence have been seen in numerical simulations of symmetrically unstable fronts run with sufficiently large domains (Skyllingstad et al., 2017; Stamper & Taylor, 2016). The SI turbulence in the simulations of Stamper and Taylor (2016) in particular was characterized by steps in buoyancy that merged and broadened over time. Similar dynamics could have been at play in the Gulf Stream and might explain the variations in step width observed between swaths.

One complicating characteristic of the symmetrically unstable front described here is the counteracting influence of temperature and salinity on the density gradient. It is possible that some of the unexpected features of the temperature staircase could be affected by this *T-S* relation. For example, the temperature steps are not always aligned with the main SST front (e.g., swath 2 in Figure 2). However, they could still be aligned with the density front, consistent with the theory of SI, if the salinity and temperature fronts were misaligned. Another interesting feature of the steps is that they do not form a perfect staircase, instead, the temperature decreases in a "cold-trough" prior to the rapid increase in temperature at each step. If the steps are caused by the convergent flow associated with the overturning circulations of SI, as in simulations of Thomas (2005), then this region of temperature decrease would be coincident with downwelling. However, because the water is cooler near the surface in the fresh filament (e.g., Figure 4) downwelling would result in cooling rather than warming and thus could explain the formation of the cold-trough. Fully understanding how these surprising features in the airborne imagery form would require numerical simulations of SI turbulence in fronts with competing temperature and salinity gradients, which to our knowledge have not been undertaken, thus motivating future study.

SI turbulence derives its energy from ocean currents and not from atmospheric forcing, and thus, the staircase seen in the infrared imagery represents a sink of kinetic energy for the circulation. Here we attempt to quantify the efficacy of this sink. Wind-forced SI extracts kinetic energy from the circulation at a rate that scales with the Ekman buoyancy flux (Thomas & Taylor, 2010; Thomas et al., 2016). Thus, a symmetrically unstable current

with kinetic energy KE will spin down over a timescale $t_{sd} \sim KE/\overline{EBF}$. Since the SI observed here is acting on the cold filament where the current is of order 0.05 m s^{-1} (inferred by integrating the thermal wind shear over the depth of the filament), and given the estimate of the Ekman buoyancy flux calculated in section 4, $t_{sd} = \mathcal{O}(1{,}000\ s)$. Such a fast spin-down time gives an indication of the efficacy of SI in draining the circulation of its kinetic energy and also suggests that this energy must be rapidly resupplied by the Gulf Stream to sustain the instability.

Acknowledgments
Funding for this research was provided by NRL program element 61153N (WUs BE023-01-41-1C04 and -6692) and ONR grant N0001416WX00469. L. N. T. was supported by NSF grant OCE-1459677. Data used in this paper are a subset of CASPER-East data set, hosted on https://researchworkspace.com/campaign/2560812/coupled-air-sea-processes-and-em-ducting-research-casper and are a subject to mandatory public release in accordance with policies established by U.S. Navy. We thank John Taylor and an anonymous reviewer for improving the article with their insightful and helpful comments and suggestions.

References

Alappattu, D. P., Wang, Q., Yamaguchi, R., Lind, R. J., Christman, A. J., & Shearman, K. (2017). Generating accurate skin sea surface temperature data from observations made using multiple platforms during casper field experiment (*Naval Postgraduate School Report*). NPS-MR-17-001.

Alappattu, D. P., Wang, Q., Yamaguchi, R., Lind, R. J., Reynolds, M., & Christman, A. J. (2017). Warm layer and cool skin corrections for bulk water temperature measurements for air-sea interaction studies. *Journal of Geophysical Research: Oceans*, *122*, 6470–6481. https://doi.org/10.1002/2017JC012688

Chen, S., Campbell, T. J., Jin, H., Gabersek, S., Hodur, R. M., & Martin, P. (2003). Effect of two-way air-sea coupling in high and low wind speed regimes. *Monthly Weather Review*, *138*, 3579–3602.

D'Asaro, E., Lee, C. M., Rainville, L., Harcourt, R., & Thomas, L. N. (2011). Enhanced mixing and energy dissipation at ocean fronts. *Science*, *15*, 318–322.

Edson, J. B., Jampana, V., Weller, R. A., Bigorre, S. P., Plueddemann, A. J., Fairall, C. W., … Hersbach, H. (2013). On the exchange of momentum over the open ocean. *Journal of Physical Oceanography*, *43*(8), 1589–1610.

Etling, D., & Brown, R. A. (1993). Roll vortices in the planetary boundary layer: A review. *Boundary-Layer Meteorology*, *65*, 215–248.

Farmer, D. M., & Li, M. (1995). Patterns of bubble clouds organised by Langmuir circulation. *Journal of Physical Oceanography*, *25*, 1425–1440.

Ferrari, R., & Wunsch, C. (2009). Ocean circulation kinetic energy: Reservoirs, sources, and sinks. *Annual Review of Fluid Mechanics*, *41*, 253–282.

Haine, T. W. N., & Marshall, J. (1998). Gravitational, symmetric, and baroclinic instability of the ocean mixed layer. *Journal of Physical Oceanography*, *28*, 634–658.

Klymak, J. M, Shearman, R. K., Gula, J., Lee, C. M., D'Asaro, E. A., Thomas, L. N., … Molemaker, J. (2016). Submesoscale streamers exchange water on the north wall of the Gulf Stream. *Geophysical Research Letters*, *43*, 1226–1233. https://doi.org/10.1002/2015GL067152

McWilliams, J. C. (2016). Submesoscale currents in the ocean. *Proceedings of the Royal Society of London A*, *472*, 1–32.

McWilliams, J. C., Sullivan, P. P., & Moeng, C. H. (1997). Langmuir turbulence in the ocean. *Journal of Fluid Mechanics*, *334*, 31–58.

Skyllingstad, E. D., Duncombe, J., & Samelson, R. M. (2017). Baroclinic frontal instabilities and turbulent mixing in the surface boundary layer. Part II: Forced simulations. *Journal of Physical Oceanography*, *47*, 2429–2454.

Smith, J. A. (1998). Evolution of Langmuir circulation during a storm. *Journal of Geophysical Research*, *103*, 12649–12668.

Smith, J. A., Pinkel, R., & Weller, R. (1987). Velocity structure in the mixed layer during MILDEX. *Journal of Physical Oceanography*, *17*, 425–439.

Stamper, M., & Taylor, J. R. (2016). The transition from symmetric to baroclinic instability in the Eady model. *Ocean Dynamics*, *67*, 65–80.

Taylor, J., & Ferrari, R. (2010). Buoyancy and wind-driven convection at a mixed-layer density fronts. *Journal of Physical Oceanography*, *40*, 1222–1242.

Thomas, L. N. (2005). Destruction of potential vorticity by winds. *Journal of Physical Oceanography*, *35*, 2457–2466.

Thomas, L. N., & Lee, C. M. (2005). Intensification of ocean fronts by down-front winds. *Journal of Physical Oceanography*, *35*, 1086–1102.

Thomas, L. N., & Taylor, J. R. (2010). Reduction of the usable wind-work on the general circulation by forced symmetric instability. *Geophysical Research Letters*, *37*, L18606. https://doi.org/10.1029/2010GL044680

Thomas, L. N., Taylor, J. R., D'Asaro, E. A., Lee, C. M., Klymak, J. M., & Shcherbina, A. Y. (2016). Symmetric instability, inertial oscillations, and turbulence at the Gulf Stream front. *Journal of Physical Oceanography*, *46*, 197–217.

Thomas, L. N., Taylor, J. R., Ferrari, R., & Joyce, T. M. (2013). Symmetric instability in the Gulf Stream. *Deep-Sea Research Part II*, *91*, 96–110.

Wang, Q., Alappattu, D. P., Billingsley, S., Blomquist, B., Burkholder, R. J., Christman, A. J., … Yardim, C. (2017). CASPER: Coupled air-sea processes and electromagnetic (EM) ducting research. *Bulletin of the American Meteorological Society*. https://doi.org/10.1175/BAMS-D-16-0046.1